Evaluation of multicontrast MRI including fat suppression and inversion recovery spin echo for identification of intra-plaque hemorrhage and lipid core in human carotid plaque usin...

ARTICLE *in* MAGNETIC RESONANCE IN MEDICINE · JUNE 2012

Impact Factor: 3.57 · DOI: 10.1002/mrm.23191 · Source: PubMed

Magnetic Resonance in Medicine 67:1764–1775 (2012)

Evaluation of Multicontrast MRI Including Fat Suppression and Inversion Recovery Spin Echo for Identification of Intra-Plaque Hemorrhage and Lipid Core in Human Carotid Plaque Using the Mahalanobis Distance Measure

Bernard C. te Boekhorst,[1]* Ronald van 't Klooster,[2] Sandra M. Bovens,[1,3] Kees W. van de Kolk,[1] Maarten J. Cramer,[1] Matthijs F. van Oosterhout,[4] Pieter. A. Doevendans,[1] Rob J. van der Geest,[2] Gerard Pasterkamp,[1] and Cees J. van Echteld[1]

Intra-plaque hemorrhage (IPH) and lipid core, characteristics of rupture prone carotid plaques, are often visualized in vivo with MRI using T1 weighted gradient and spin echo, respectively. Increasing magnetic field strength may help to identify IPH and lipid core better. As a proof of concept, automatic segmentation of plaque components was performed with the Mahalanobis distance (MD) measure derived from image contrast from multicontrast MR images including inversion recovery spin echo and T1 weighted gradient echo with fat suppression. After MRI of nine formaldehyde-fixated autopsy specimens, the MDs and Euclidean Distances between plaque component intensities were calculated for each MR weighting. The distances from the carotid bifurcation and the size and shape of calcification spots were used as landmarks for coregistration of MRI and histology. MD between collagen/cell-rich area and IPH was largest with inversion recovery spin echo (4.2/9.3, respectively), between collagen/cell-rich area/foam cells and lipid core with T1 weighted gradient echo with fat suppression (26.9/38.2/4.6, respectively). The accuracy of detection of IPH, cell-rich area, and collagen increased when the MD classifier was used compared with the Euclidean Distance classifier. The enhanced conspicuity of lipid core and IPH in human carotid artery plaque, using ex vivo T1 weighted gradient echo with fat suppression and inversion recovery spin echo MRI and MD classifiers, demands further in vivo evaluation in patients. Magn Reson Med 67:1764–1775, 2012. © 2011 Wiley Periodicals, Inc.

Key words: MRI; rupture prone plaque; intra-plaque hemorrhage; lipid core

Clinically, the degree of stenosis, which is generally identified by angiography, is often used as a marker for plaques that may give rise to clinical symptoms. However, lumenography is regarded to be insufficient for identification of vulnerable plaques for two reasons. Outward remodeling with preservation of lumen size is a characteristic of vulnerable plaques but cannot be identified with lumenography (1). Second, plaque composition rather than lumen size appears to determine plaque vulnerability. For identification of high-risk carotid artery plaque not only the classical markers of plaque vulnerability-large lipid core (LC), a thin fibrous cap (2), and abundance of macrophages (3) but also intra-plaque hemorrhage (IPH) has been recognized as an important predictor of major clinical events, e.g., transient ischemic attack or stroke (4–6). MRI is the most promising technique for visualization of these plaque markers, because each plaque component generates unique MR contrast in various MR acquisitions, the technique is noninvasive and depicts the anatomy of the vessel. A substantial number of studies have been reported on carotid artery plaque MRI both ex vivo (7–11) and in vivo (4,5,12–15). In most studies, multicontrast weighted MRI is used for characterization of carotid atherosclerotic plaque. In particular, reports have stressed the importance of T2 weighted (T2w) spin echo (SE) sequences for differentiation between LC and fibrous tissue (7). More recently, T1 weighted fast SE and gradient echo (GE) imaging have gained interest, because these sequences may lead to better visualization and bright depiction of IPH (4–6) and LC(12,16,17).

With the advent of clinical high field magnets (7 T), interest in the possibilities for in vivo carotid artery imaging at high field strength has grown. Higher field magnets bring the advantage of increased SNR or the possibility to increase resolution. Unfortunately, adjustments to MR sequences or development of novel methods are necessary, as T1 of a particular tissue increases with increasing field strength, while T2 decreases, necessitating adjustment of MR sequences to generate optimized contrast. Inversion Recovery Spin Echo (IR-SE) has a larger potential for visualization of T1 differences than nonprepared T1 weighted SE or GE (18). Possibly,

[1]Department of Cardiology, University Medical Center Utrecht, Utrecht, Netherlands.

[2]Division of Image Processing, Department of Radiology, Leiden University Medical Center, Leiden, Netherlands.

[3]Interuniversity Cardiology Institute of the Netherlands, Utrecht, Netherlands.

[4]Department of Pathology, University Medical Center Utrecht, Utrecht, Netherlands.

Grant sponsor: Netherlands Heart Foundation; Grant number: 2003B249.

*Correspondence to: Bernard C. te Boekhorst, Experimental Cardiology Laboratory, Division Heart and Lungs, G02.523, 3584CX, Utrecht, The Netherlands. E-mail: b.t.boekhorst@tue.nl

Received 7 March 2011; revised 27 July 2011; accepted 30 July 2011.

DOI 10.1002/mrm.23191

Published online 13 October 2011 in Wiley Online Library (wileyonlinelibrary.com).

Table 1
MR Acquisition Parameters

MR weighting	T1w GE	T1wFS GE	PDw FSE	T2w FSE (intermediate TE)	T2w FSE (long TE)	IR-SE (TI = 400 ms)	IR-SE (TI = 1000 ms)	IR-SE (TI = 1300 ms)
TR (ms)	300	300	3500	3500	3500	5000	5000	5000
TE (ms)	2.14	2.14	8.53	19.76	37.97	3.10	3.10	3.10
ETL	–	–	8	16	16	–	–	–
Flip angle (°)	60	60	90/180	90/180	90/180	90/180	90/180	90/180
Inversion time (ms)	–	–	–	–	–	400	1000	1300
FOV (mm × mm)	10 × 10	10 × 10	10 × 10	10 × 10	10 × 10	10 × 10	10 × 10	10 × 10
Matrix	256 × 256	256 × 256	256 × 256	256 × 256	256 × 256	256 × 256	256 × 256	256 × 256
Resolution (μm × μm)	39 × 39	39 × 39	39 × 39	39 × 39	39 × 39	39 × 39	39 × 39	39 × 39
Thickness (mm)	0.5	0.5	0.5	0.5	0.5	0.5	0.5	0.5
Number of slices	20	20	20	20	20	1	1	1
Bw (kHz)	152	152	152	152	152	200	200	200
Fat suppression	–	+	–	–	–	–	–	–
NEX	50	50	50	50	50	6	6	6
AT (h:mm:ss)	1:04:00	1:04:00	1:33:20	0:46:40	0:46:40	2:08:00	2:08:00	2:08:00

ETL: echo train length; FOV: field of view; Bw: bandwidth; NEX: number of excitations; AT: acquisition time.

sharp delineation of IPH, characterized by short T1, and differentiation from adjacent stable plaque components at higher field will be better with the IR-SE technique than with the nonprepared SE or GE technique.

Additionally, early studies have revealed that chemical shift imaging of lipid, aimed at the narrow frequency range of methylene protons within adipose tissue, could visualize LC (19,20). At 9.4 T, T1 weighted GE with chemically selective fat suppression (FS), aimed at the same frequency range as in the mentioned studies, allowed for better delineation of LC then T1 weighted GE without this FS (21).

To objectively compare the image contrast between different plaque components amongst different MR sequences, techniques are needed that can quantify image contrast, based on absolute signal levels, which may vary across platforms and with coil configurations. Moreover, such statistical measures can be used in conjunction with pattern recognition techniques to enable automatic segmentation of plaque components based on their signal characteristics. In a number of studies, the Euclidean Distance (ED) measure is used for identification of plaque components (9). An important drawback of the ED is that the measure cannot be used to compare differently scaled signals from different domains (in this particular case: contrast weightings). The Mahalanobis Distance (MD) measure is scale-invariant and takes into account correlation of the data (22,23), enabling comparison of image contrast between different MR sequences.

The first objective of this study is to investigate the added value of IR-SE and T1 weighted GE with FS (T1wFS) to multicontrast weighted MRI at high field for identification of unstable plaque components.

The second objective of this study is to compare the MD to the ED between various human carotid plaque components on various MR weighted images. We hypothesize that automated plaque classification using a MD measure may result in improved assessment of plaque components, when compared with the ED measure.

MATERIALS AND METHODS

MRI

Nine carotid artery specimens (including bifurcation), obtained at autopsy, were 4% formaldehyde fixated and stored at 4°C for at least 48 h. Samples were rewarmed to 37°C before and kept at 37°C during imaging. This set of carotid artery specimens was used as the study set.

The artery samples were imaged in a vertical 9.4 T, 89 mm bore size magnet equipped with 1500 mT/m gradients and connected to an Avance 400 MR system (Bruker BioSpin, Ettlingen, Germany) using a quadrature-driven birdcage coil with an inner diameter of 10 mm. Care was taken to remove any air bubbles.

During a couple of pilot experiments at 9.4 T inversion time (TI) was varied and contrast between regions which were assumed to contain collagen (fibrous cap) and regions which were assumed to contain IPH was optimized, while nulling the regions which were assumed to contain collagen. After some cycles of optimization, these imaging results corresponded with histology. The same holds true for the chosen pulse repetition time (TR) for the T1w GE and the echo time (TE) for the T2w fast spin-echo sequence. During these pilot experiments, we found that contrast on T1w fast spin echo (FSE) showed no contrast difference, when compared with T2w FSE with intermediate TE. Therefore, we performed T1w GE which showed apparently different contrast. Eventually, we came up with the next panel of six MR sequences: T1 weighted GE with (T1wFS) and without FS (T1w), proton density weighted (PDw), FSE, T2w FSE with intermediate and long TE and IR-SE. For all acquisition parameters, see Table 1.

T1 and T2 Measurements of Fresh and Formaldehyde 4%-Fixated Femoral Artery Plaque

The T1 and T2 measurements were arranged to compare T1 and T2 values of plaque components of fresh plaque to formaldehyde-fixated plaque and because of the large

differences between reported plaque component T1 and T2 values. Thus, we aimed at useful application of sequences to the clinical in vivo situation at ultra-high field. Adjustment of in vitro protocols to the in vivo situation could be based on the differences in T1 and T2 between fresh and formaldehyde-fixated material. For this reason, we performed T1 and T2 measurements on fresh femoral artery plaque components both before and after formaldehyde fixation. Three diseased femoral arteries were freshly obtained following surgery, immediately warmed to 37°C and imaged. T1 was obtained from a series of IR images with increasing TIs (20 ms–8000 ms) and a TR of 9500 ms. T2 was obtained from a series of images obtained with a single-slice multiecho imaging sequence with incremented TEs (4–100 ms) and a TR of 5000 ms. After T1 and T2 measurements (duration 2 h), samples were formaldehyde 4% fixated, stored at 4°C. Forty-eight hours later, T1 and T2 measurements were repeated at exactly the same slice position using visual landmarks based on plaque and wall morphology.

Histology

Carotid and femoral artery specimens were decalcified by submersion in ethylenediaminetetra-acetic acid for 24 h and embedded in paraffin. A total of 10 μm axial sections were cut at 0.5 mm intervals. Hematoxylin & eosin and collagen stainings with Picrosirius red were performed. Photographs of stained slices (jpeg format) and MR data (ParaVision 4.0 (Bruker Biospin, Ettlingen, Germany) converted to DICOM format) were manipulated with ImageJ software (W. Rasband, version 1.29, National Institutes of Health, Bethesda, Maryland, USA). On every histological slice for each recognizable plaque component, a region of interest (ROI) was traced. All histological slices were evaluated by a research physician experienced in histopathology, and unambiguous ROIs representing the following plaque components ("truth regions"), were delineated: LC, IPH, collagen, cell-rich area, foam cells, and calcification. Necrotic areas with cholesterol crystals were identified as LC. Areas with (remnants of) erythrocytes and fibrin strands on Hematoxylin & eosin staining were identified as IPH. Closely packed spindle-shaped cells and high densities of nuclei (both smooth muscle cells and fibroblasts) in the fibrous cap of plaque were identified as cell-rich areas. Closely packed purple/red strands on Picrosirius Red staining were identified as collagen. Lipid-laden round cells on Hematoxylin & eosin staining were identified as foam cells.

Image Processing and Manual Image Segmentation

Image segmentation was performed using histology assisted tracing with VesselMass software (LKEB, Leiden, Netherlands) and subsequently statistical analysis was performed using Matlab (The Mathworks, Natick, Massachusetts, USA). The truth regions served as user input and represent the various "classes" or plaque components.

We used the distance from the carotid bifurcation and the luminal shape and unique morphology and size of calcification spots as visual landmarks for longitudinal matching of MRI with histology. The luminal shape and morphology and size of calcification spots were used for correction of orientation and axial matching of MRI with histology. Twenty-three histological carotid artery sections and six femoral artery sections could be matched to MR images. After correction of orientation, ROIs were copied from histological images to longitudinally matching MRI slices and proportionately upscaled to MR images, accounting for both deformation in the x and y direction in the axial plane. For MR images of femoral artery plaque representing the T1 and T2 measurement data sets, the mean absolute signal intensities of the ROIs were plotted against TI or TE. Mono-exponential recovery functions were fitted to the T1 data sets and mono-exponential decay functions were fitted to the T2 data sets to obtain the T1 and T2 values, respectively.

Calculation of MD

Quantitation of image contrast between different plaque components can be achieved by calculating the intensity-based distance between the two classes. For each MR sequence, the signal intensities of the various plaque components were determined, and the distance was calculated for all available pairs of plaque components. In this study, the MD metric is used. MD measures the separation of two groups of objects and takes into account correlations of the data set (Fig. 1a,b). Moreover, it is scale-invariant (Fig. 1a,c), so tissue-independent variation of the MR signal will not affect MD and MD may allow for differentiation of classes based on variably scaled parameters created by different imaging modalities.

The plaque region is described by a group of image locations (pixels). For each pixel, the signal intensities of multiple MR sequences are available. So, each image pixel x corresponds to a vector containing the signal intensities of the different MR sequences. The MD between two plaques, i.e., groups X_i and X_j with group means x_i^- and x_j^-, is given as a matrix calculation in Eq. 1. X_i contains all image pixels x of group i.

$$(\mathrm{MD}_{ij})^2 = (x_i^- - x_j^-)^{\mathrm{T}} S^{-1} (x_i^- - x_j^-) \quad [1]$$

where:

T = matrix transpose

S^{-1} = Inverse of the pooled covariance matrix of the two groups; this matrix is computed as the weighted average of the two covariance matrices.

As a reference, the equation of the ED between two groups is given:

$$(\mathrm{ED}_{ij})^2 = (x_i^- - x_j^-)^2 \quad [2]$$

MDs of all selected ROIs were pooled per weighting and per pair of components. The MR weighting leading to the highest pooled MD was determined for pairs of plaque components including both an established stable and unstable plaque component (lipid core-cell rich area, lipid core-collagen, IPH-cell rich area, IPH-collagen, foam cells-cell rich area, and foam cells-collagen) and for the pair lipid core-foam cells.

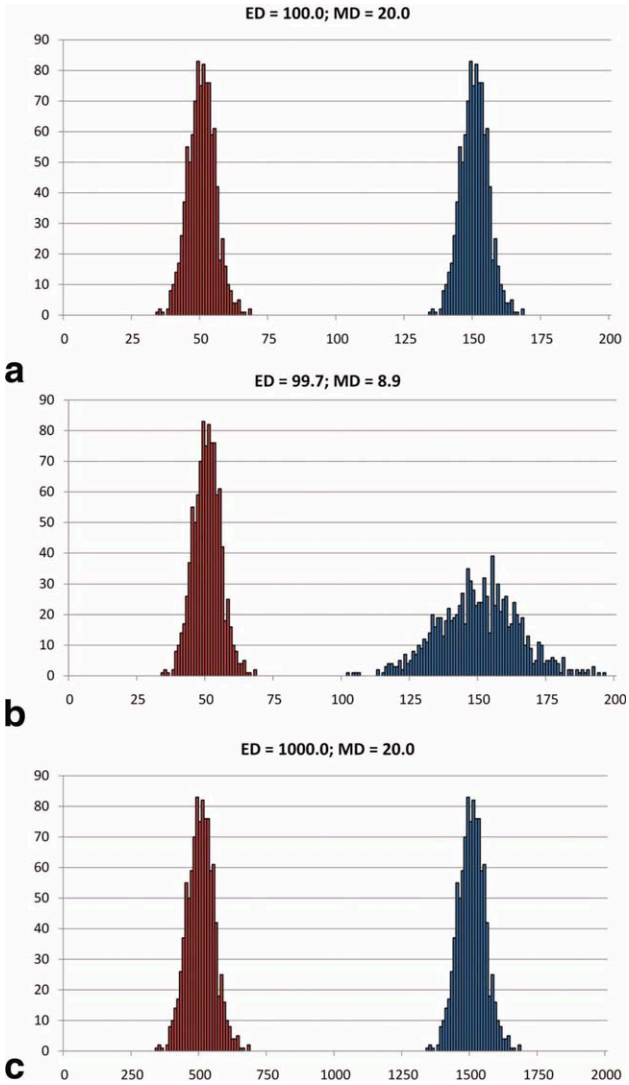

FIG. 1. The influence of the distribution width (**a** versus **b**) and scaling (a versus **c**) of artificial data with a normal distribution on MD and ED. [Color figure can be viewed in the online issue, which is available at wileyonlinelibrary.com.]

Automatic Segmentation of Plaque Components

Three carotid artery samples were used to perform two segmentation experiments. In these experiments, a MD classifier and an ED classifier were used to segment plaque areas. The classifier was trained by the histology assisted traced truth regions.

1. Each carotid artery sample consisted of four slices. A Mahalanobis (22) and an Euclidean classifier were trained on three slices and then applied to the fourth slice for automatic segmentation of the plaque components on a pixel-by-pixel basis. This process was repeated for each carotid artery sample resulting in three automatically segmented slices (one for each carotid artery sample).
2. The slices of the three carotid arteries, in total 12 slices, were pooled to create a training set of 11 slices and a test set of one slice. Again, a Mahalanobis and an Euclidean classifier were trained and applied on the test set. For each carotid artery sample, the slice of the test set was chosen to be the same slice as used in experiment one, but the training set consisted of the other 11 slices. This experiment also resulted in three automatically segmented slices.

An automatic plaque classification experiment with a training set that is fully independent of the test set was not possible due to the limited number of carotid samples containing sufficient plaque components. Segmentation results from both experiments were compared because in both experiments, the same slices were used as test set.

These procedures were executed for various relevant combinations of MR weightings, including T1w/T2w/PDw, (T1wFS/T2w/PDw), T1w/T2w/PDw/IR-SE, T1w/T2w/PDw/T1wFS, and T1w/T1wFS/T2w/PDw/IR-SE.

Sensitivity, Specificity, Accuracy

The results of the automatic segmentation were compared on a pixel-by pixel basis to the truth regions of the corresponding slice. Segmentation results from the three carotid artery samples were averaged for each experiment to determine the sensitivity and specificity of the classifier for each plaque component. Sensitivity is defined as: the number of pixels correctly labeled by the classifier as tissue x (true positive pixels) divided by the total number of pixels labeled tissue x as determined by histological review. The percentage false negative pixels is (100 − sensitivity(%)). Specificity is defined as the number of pixels correctly excluded by the classifier from tissue x (true negative pixels) divided by the total number of pixels excluded from tissue x as determined by histological review. The percentage false positive pixels is (100 − specificity(%)). The accuracy was calculated as the total number of pixels correctly labeled by the classifier divided by the total number of pixels analyzed.

RESULTS

T1 and T2 Measurements of Fresh and 4% Formaldehyde Fixated Plaque

T1 and T2 values measured in fresh and 4% formaldehyde fixated plaque are listed in Table 2. T2 values of all components in freshly obtained plaque were shorter when compared with 4% formaldehyde fixated plaque. T1 values of all components in freshly obtained plaque were longer when compared with 4% formaldehyde fixated plaque.

Visual Inspection of MRI of Carotid Plaque

LC and IPH are visualized best with T1wFS and IR-SE, respectively (Figs. 2 and 3). T1wFS creates largest contrast between LC (dark) and other plaque components including foam cells (brighter). IR-SE shows largest contrast between IPH (bright) and other plaque components (darker).

Table 2
T1 and T2 Values of Fresh and 4% Formaldehyde-Fixated Atherosclerotic Human Femoral Artery Plaque Components at 9.4 T and at 37°C

Plaque component	Fresh in PBS T1 (ms)	4% formaldehyde-fixated T1 (ms)	Fresh in PBS T2 (ms)	4% formaldehyde-fixated T2 (ms)
IPH (old)	827 ± 296	793 ± 158	4.6 ± 0.11	10.9 ± 2.30
IPH (recent)	982 ± 246	833 ± 139	12.1 ± 1.05	15.0 ± 2.15
Lipid core	1110 ± 171	1035 ± 105	10.6 ± 1.97	13.3 ± 2.40
Foam cells	1230 ± 300	1150 ± 62	12.4 ± 1.88	17.4 ± 2.91
Cell rich area	1538 ± 386	1446 ± 41	28.9 ± 3.81	33.4 ± 4.72
Collagen	1578 ± 440	1548 ± 88	25.6 ± 5.82	30.3 ± 3.12

PBS: phosphate buffered saline.
Data are expressed as mean ± SD of three measurements of three sets of components from three plaques. Thrombus was only encountered in one of these plaques.

Calculation of the MD

Figure 4 shows the mean absolute signal intensities of the ROIs corresponding with plaque components for various carotid artery samples. Samples show large variations of intensities per plaque component and per MR weighting. The diversity of composition of an agreed distinct plaque component like LC or IPH, additional to day-to-day differences of shim settings may cause these variations. However, the relative intensity differences between plaque components are similar per MR weighting (Fig. 4).

Calcification has low signal intensity on all MR weightings. IPH has high signal intensity on IR-SE (TI = 1000 ms) images, while other plaque components show lower signal intensities on these images. Cell-rich areas

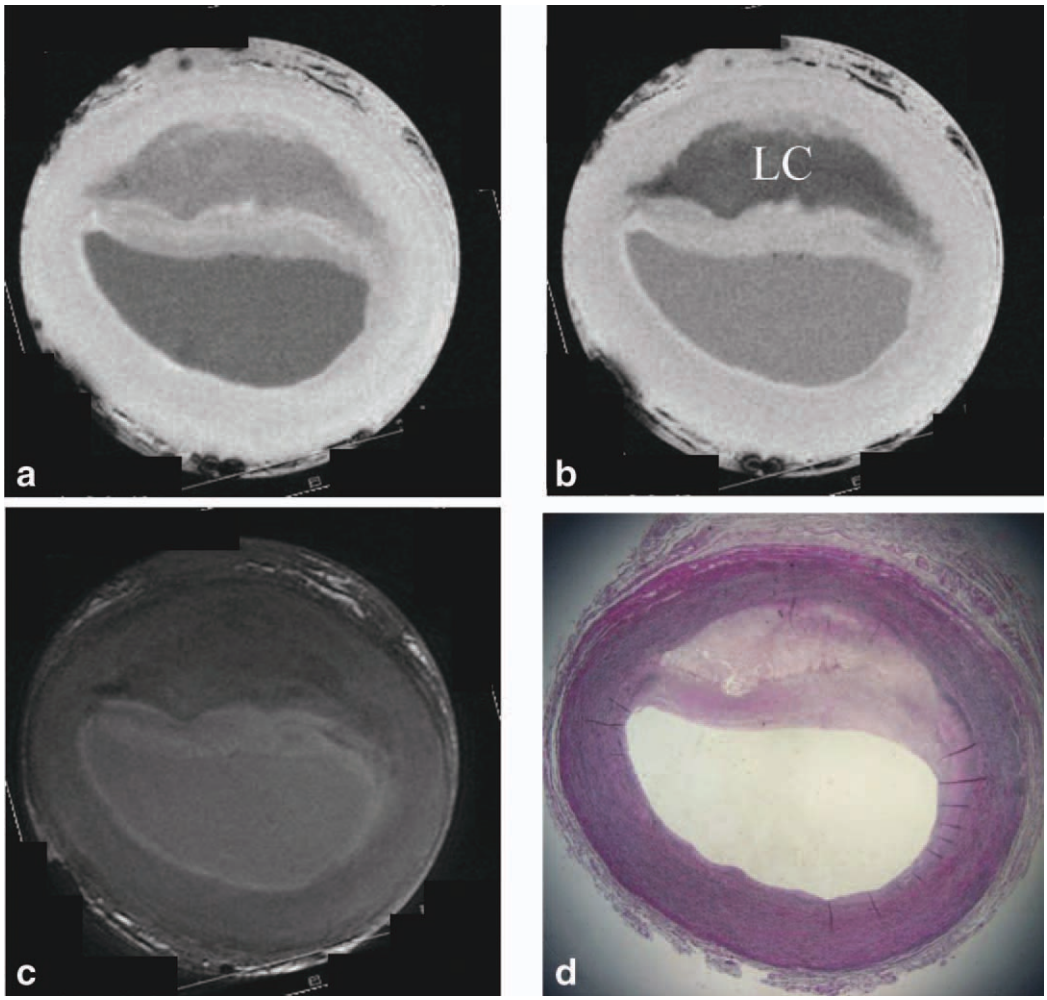

FIG. 2. MRI and histology of carotid artery plaque with a large LC: (**a**) T1w, (**b**) T1wFS, (**c**) T2w, and (**d**) EVG staining. Conspicuity of LC is enhanced on T1wFS, when compared with T1w. LC = LC.

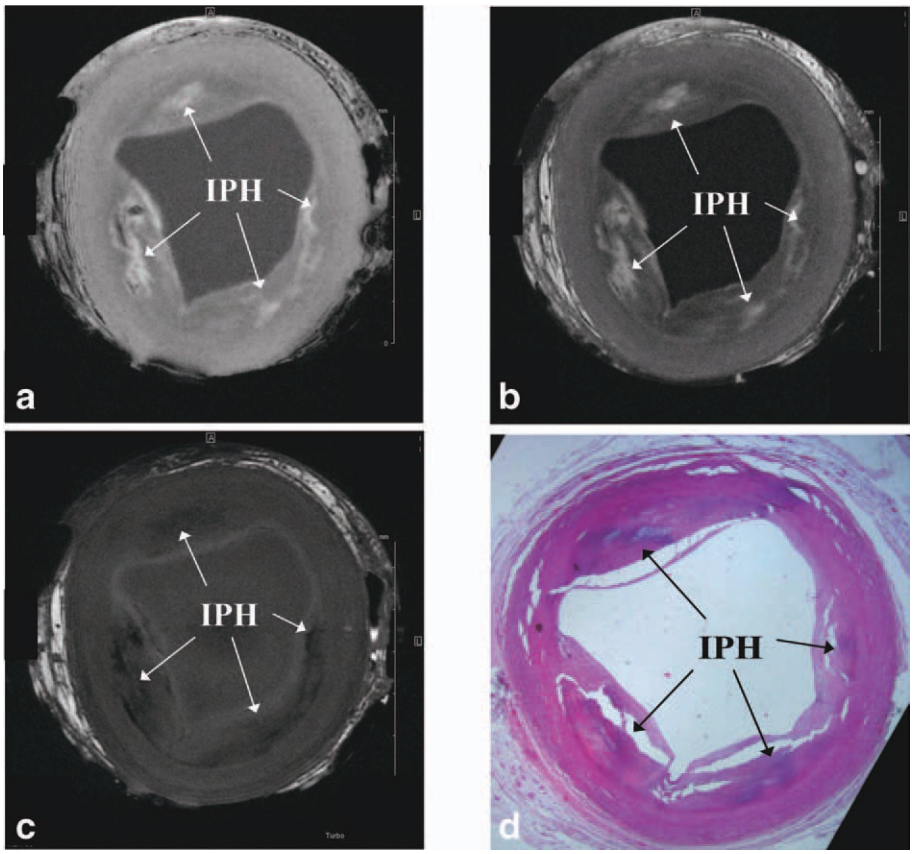

FIG. 3. MRI and histology of human carotid atherosclerotic plaque with multiple regions of IPH: (**a**) T1w, (**b**) IR-SE (TI = 1000 ms), (**c**) T2w with intermediate TE, and (**d**) Hematoxylin & eosin staining. Arrows indicate IPH. T1w and IR-SE image show bright regions in the plaque corresponding with IPH. IPH on T2w image is dark. IR-SE image shows highest contrast of IPH.

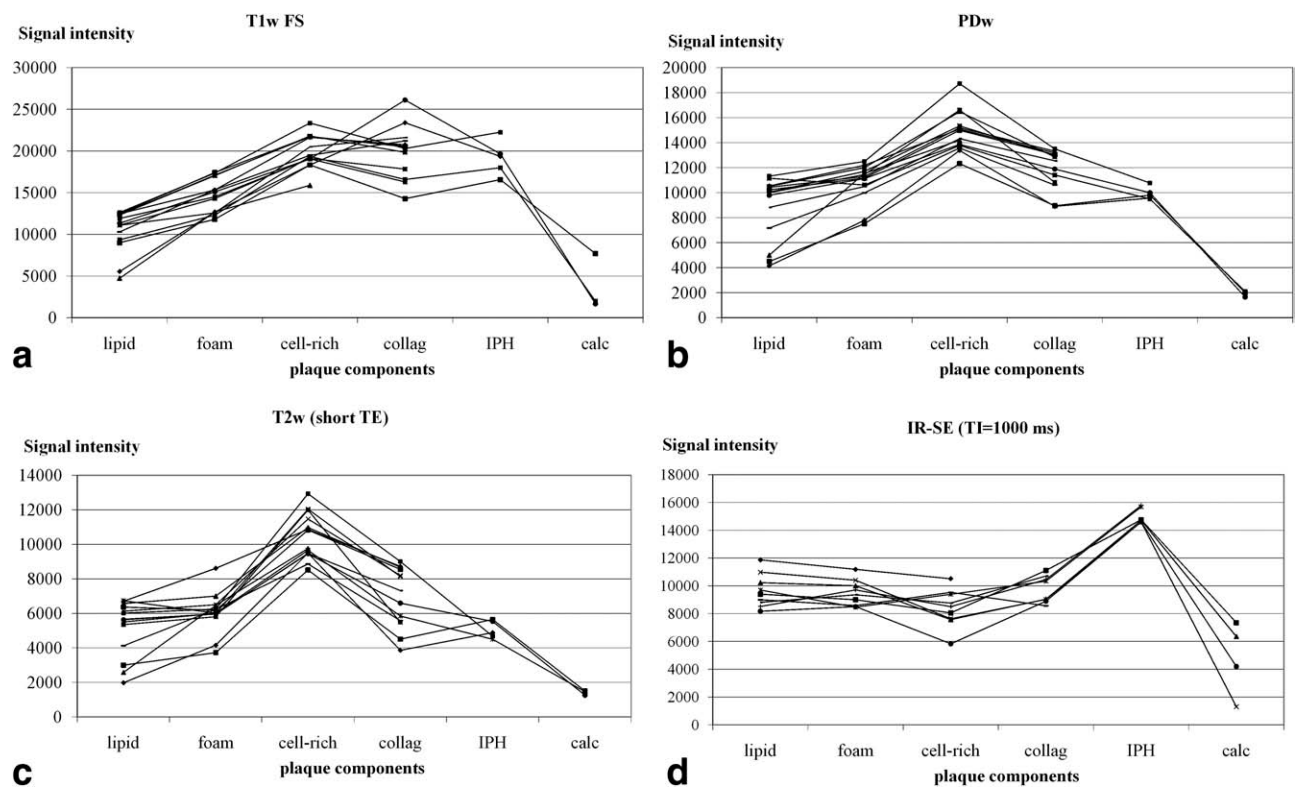

FIG. 4. Absolute signal intensities (*y*-axis) of various components (*x*-axis) on T1wFS (**a**), PDw images (**b**), T2w with intermediate TE (**c**), and IR-SE (with TI = 1000 ms) (**d**) images.

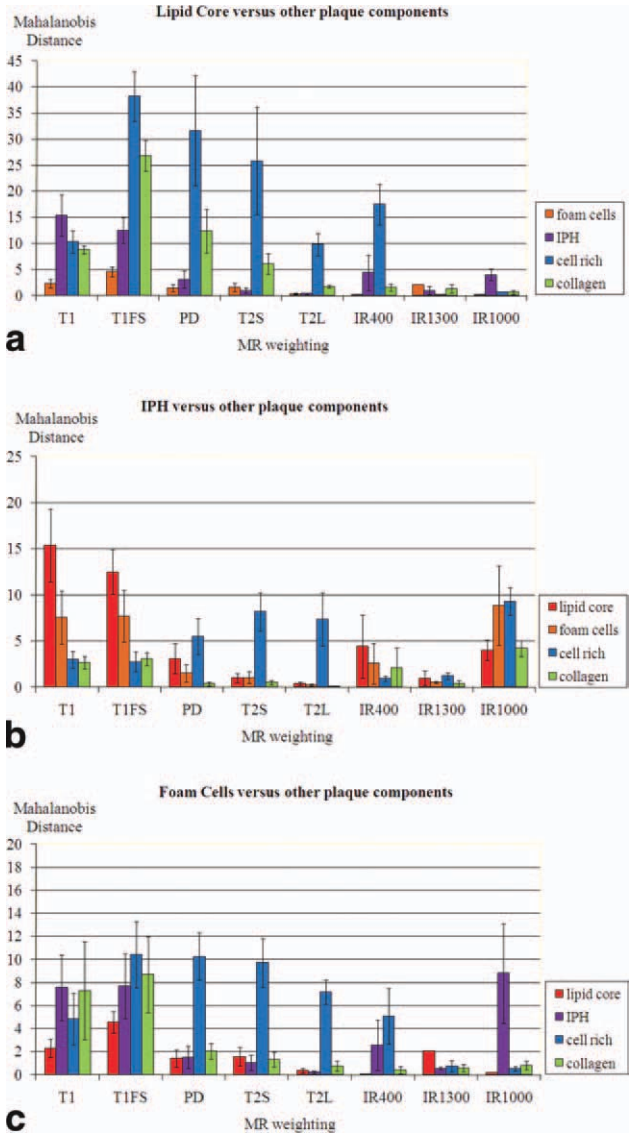

FIG. 5. MD between vulnerable carotid plaque components and stable plaque components. **a**: MD between LC and IPH, foam cells, cell rich areas, collagen. **b**: MD between IPH and LC, foam cells, cell rich areas, collagen. **c**: MD between foam cells and LC, IPH, cell rich areas, collagen.

have high signal intensity on PDw images, while other plaque components have lower signal intensities on these images.

On every histological slice for each recognizable plaque component, a ROI (truth region) was traced, and the mean signal intensities for the ROIs were calculated for each of the different MR contrast weightings. By calculating the MD for each pair of plaque components per MR weighting, a characteristic signature for each plaque component could be determined. Pooled MDs are shown in Figure 5. IR-SE with TI = 1000 ms leads to larger MD between collagen or cell-rich area and IPH (4.2 and 9.3, respectively), when compared with other MR sequences. T1wFS appears to lead to larger MD between LC and foam cells or cell rich areas or collagen (4.6, 38.2, and 26.9, respectively), when compared with the other sequences (Fig. 5).

An example of discrimination between lipid, cell rich area, and collagen using both the ED and the MD is shown in Fig. 6. In the presented case, the MD is better able to discriminate between different plaque components than the ED. Consequently, in this particular case, the MD metric is preferred to the ED.

Figure 7 shows the correspondence of truth regions and automatically segmented regions in one carotid artery sample after training on three, the first segmentation experiment, and after training on 11 pooled slices, the second segmentation experiment.

The sensitivity/specificity/accuracy of detection of various plaque components (LC, IPH, cell rich area, and collagen) achieved with various sets of MR weightings is reported in Table 3 for the first segmentation experiment, and Table 4 for the second segmentation experiment, using both the MD- and ED-based classifier.

Segmentation Results, First Experiment

Large LC in the absence of IPH was easily distinguished with T1w, T2w, and PDw imaging, while the sensitivity of the detection of LC in the presence of IPH was greatly improved by replacement of T1w with T1wFS and addition of IR-SE to the standard clinical set of MR weightings (T1w, PDw, and T2w) (Table 3). No differences between results of the first segmentation experiment obtained with ED and MD classifiers were found (Table 3).

Segmentation Results, Second Experiment

Combination of T1wFS with T2w improved the sensitivity, specificity, and accuracy of the detection of LC, when compared with the standard clinical set. The specificity and accuracy of the detection of IPH were improved by the combination of T1w, T2w, PDw, and IR-SE, when compared with the standard clinical set. Sensitivity was improved by replacement of T1w with T1wFS and addition of IR-SE to the standard set of MR weightings. Sensitivity and accuracy were improved by replacement of T1w with T1wFS and addition of IR-SE to the standard set of MR weightings (T1w, PDw, and T2w), with only a minor decrease of specificity. Sensitivity of the detection of collagen was improved by addition of both T1wFS and IR-SE to the standard set of MR weightings (T1w, PDw, and T2w) (Table 4).

When the MD classifier in combination with the novel sequence panels was used, the accuracies of detection of IPH, cell-rich area, and collagen were greatly improved with comparable accuracy of detection of LC, when compared with application of the ED classifier (Table 4).

DISCUSSION

With respect to the first objective of this study, we show that addition of IR-SE to a panel of MR weighted sequences (T1w GE, PDw FSE, and T2w FSE) leads to better discrimination between IPH and stable plaque components of formaldehyde-fixated human carotid artery plaque. The addition of FS to T1w GE leads to better discrimination between LC and stable plaque components,

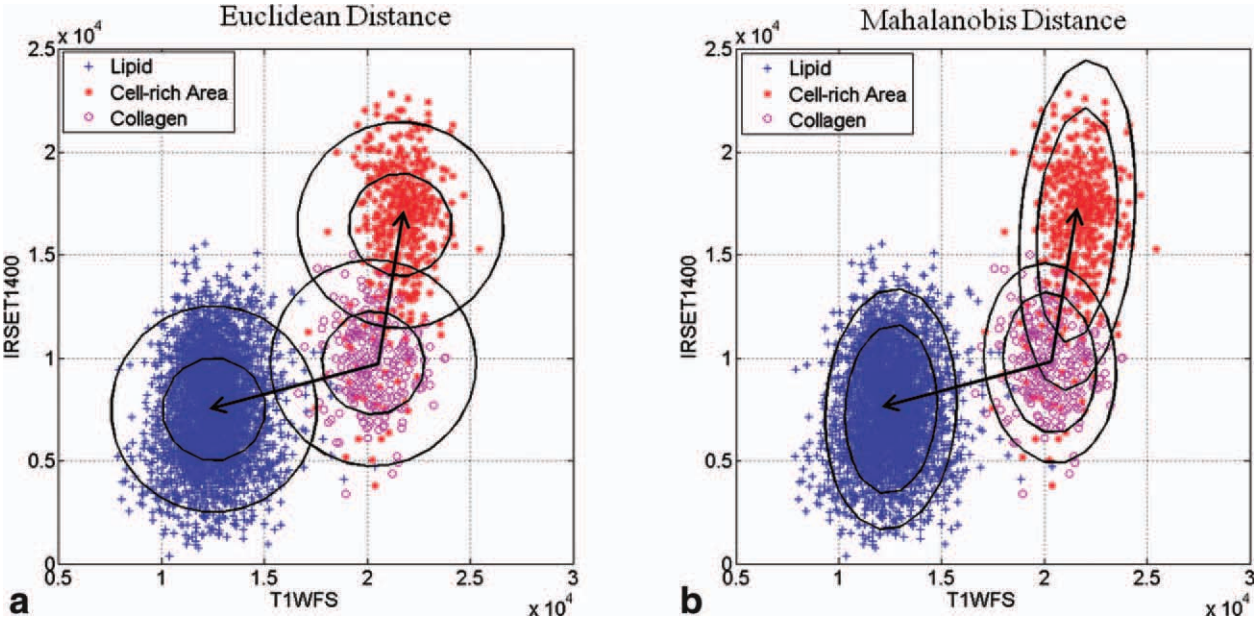

FIG. 6. ED versus MD of a cloud of data points representing collagen. Each data point represents a pixel. The ED does not take into account the correlation of the data points according to the circular form of the iso-distance lines (**a**), whereas MD does take into account the correlation of the data points according to the ellipse form of the iso-distance lines (**b**). The distances between the group centers of collagen and cell rich area and between the group centers of collagen and LC (arrows) represent EDs (a and b). The two EDs measured from collagen to LC and from collagen to cell rich area are nearly similar (a). However, the MD between collagen and LC is larger than the MD between collagen and cell rich area as can be observed from the iso-distance lines in b.

including foam cells, when compared with T1w GE without FS.

With respect to the second objective, we have performed two segmentation experiments to compare the MD to the ED between various human carotid plaque components on various MR weighted images. The first experiment shows no superiority of the MD classifier over the ED classifier. Taking into account the advantage of scale-invariance, it will not be a surprise that when the training set belonged to the same carotid artery sample as the test set, no differences between using MD or ED were found.

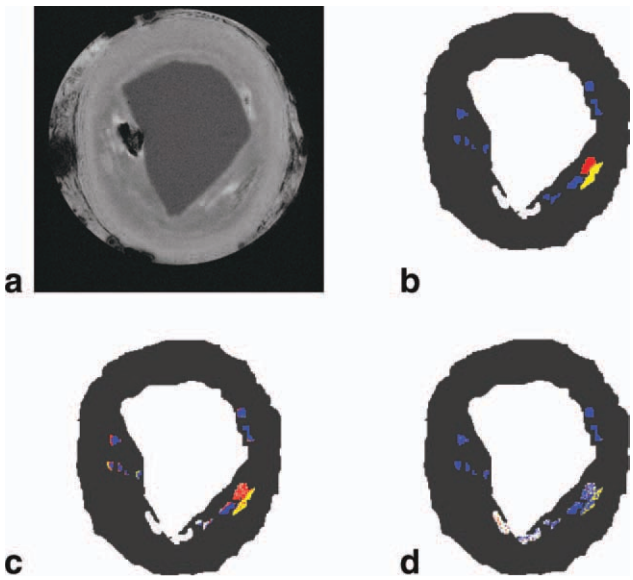

FIG. 7. **a**: MR image at one slice level of a carotid artery sample. **b**: Truth regions drawn on histology and projected to the MR image in (a, **c**). Plaque components assigned to same regions based on the first automatic segmentation experiment and (**d**) based on the second segmentation experiment on a pixel-by-pixel basis by a trained classifier (see text for additional information). Each color represents a different plaque component. Blue: IPH; red: collagen; white: cell rich area; yellow: LC.

The second segmentation experiment reveals that, in case of a partially independent training set, the suggested novel panels of sequences show higher accuracies of detection of IPH, cell-rich area, and collagen using the MD classifier than using the ED classifier. No difference in accuracy was found for the detection of LC.

To our knowledge, a head-to-head comparison between MD and ED classifiers for plaque classification from multicontrast MRI has not been reported. Automated segmentation with the "Mahalanobis distance-based classifier" provides the possibility to categorize characteristics of atherosclerotic plaques in six components. This MD-based classifier is a supervised classification algorithm, which calculates in this study the MD from multicontrast weighted ex vivo MR images. Two segmentation experiments were performed. In general, the results for the segmentation based on a training set of three slices from the same carotid artery were slightly better than the experiment where 11 slices from three carotid artery samples were pooled. However, except for the sensitivity of detection of IPH and collagen, results of segmentation using the pooled training set approximate the high values obtained with the first segmentation experiment closely.

Table 3
Sensitivity, Specificity, and Accuracy of the First Segmentation Experiment (see Text for Details) of Various Plaque Components Achieved With Various Sets of MR Weightings Using a Mahalanobis Distance- and an Euclidean Distance-Based Classifier

		Mahalanobis distance			Euclidean distance		
Plaque component	Set of MR weightings	Sensitivity (%)	Specificity (%)	Accuracy (%)	Sensitivity (%)	Specificity (%)	Accuracy (%)
Lipid core in presence of IPH	T1w/PDw/T2w	75	99	95	76	99	95
	T1wFS/PDw/T2w/IRSE	81	98	95	81	98	95
Large lipid core in absence of IPH	T1w/PDw/T2w	100	99	100	99	99	99
	T1wFS/PDw/T2w/IRSE	100	99	100	99	99	99
IPH	T1w/PDw/T2w	56	97	82	56	97	82
	T1w/PDw/T2w/IRSE	57	97	82	57	97	82
Cell-rich area	T1w/PDw/T2w	87	92	91	89	94	94
	T1wFS/PDw/T2w	89	92	92	91	95	94
Collagen	T1w/PDw/T2w	82	79	80	87	86	86
	T1w/PDw/T2w/IRSE	82	81	82	86	87	87

T1 and T2 of Plaque Components

The increase of T1 of tissues with increasing field strength increases the challenge to visualize T1 differences between plaque components at high field. Adjustment of MR sequences to increased field strengths should be based on T1 and T2 values of tissues of interest at those field strengths. However, there are some conflicting data from various reports on the T1 and T2 values of atherosclerotic plaque components at 9.4 T (7,24). Second, previous reports have shown that room temperature and formaldehyde fixation lead to important T2 changes of fibrous plaque (23). Unfortunately, for this study, fresh atherosclerotic plaque material was not sufficiently available. We compared T1 and T2 values of femoral plaque components obtained from surgery, measured at 37°C before and after 4% formaldehyde fixation. The large range of T2 values found in literature for a particular plaque component may relate to differences in definition of plaque components on histology and the procedure of T1 and T2 measurement (spectroscopic or using MR imaging) (10,17,25,26).

IPH

Differentiation between IPH and stable plaque components, though possible when using T1 weighted MR imaging without inversion-preparation, remains difficult according to the moderate specificity of 74% for the in vivo identification of recent IPH in literature (4) which is comparable with this study (specificity 71%) when using the standard set of MR weightings (T1w, PDw, and T2w). However, combination of T1w with inversion recovery SE in this study resulted in an improvement of the specificity by 14%. At 9.4 T, thrombus (= old IPH) T1 was reported to be 1180 ms, whereas T1 of fibrous tissue was reported to be ~ 1800 ms (24). Application of a method, which is more heavily T1 weighted, like inversion recovery SE could identify IPH with higher specificity. We achieved in this study clear identification of thrombus with inversion recovery SE, as a result of efficient nulling of the signal from stable plaque components. In vivo thrombus imaging has been achieved previously with a T1w inversion recovery 3D GE sequence at 1.5 T (27,28). However, choices which are made in the in vivo situation will be different when compared to the ex vivo situation and the TI in those studies was chosen to null the blood signal at 1.5 T (27,28), leaving suboptimal contrast between IPH and stable plaque components.

Lipid Core

The second component of interest in this study was LC. MRI of LC has shifted from direct lipid imaging with spectroscopic techniques (19,20) to MRI of the water signal of LC (29). T1/T2w GE (TR = 35 ms) images at 1.5 T have been reported to show iso- to hyper-intensity of LC (16,30), but T1w GE images (TR = 300 ms) at 9.4 T have

Table 4
Sensitivity, Specificity, and Accuracy of the Second Segmentation Experiment (see Text for Details) of Various Plaque Components Achieved With Various Sets of MR Weightings Using a Mahalanobis Distance- and an Euclidean Distance-Based Classifier

		Mahalanobis distance			Euclidean distance		
Plaque component	Set of MR weightings	Sensitivity (%)	Specificity (%)	Accuracy (%)	Sensitivity (%)	Specificity (%)	Accuracy (%)
Lipid core	T1w/PDw/T2w	79	82	83	63	97	90
	T1wFS/T2w	91	90	91	66	99	93
IPH	T1w/PDw/T2w	49	71	65	50	55	56
	T1w/PDw/T2w/IRSE	50	78	70	50	61	60
Cell-rich area	T1w/PDw/T2w	45	98	84	35	100	84
	T1wFS/PDw/T2w/IRSE	75	95	91	33	100	84
Collagen	T1w/PDw/T2w	44	88	84	65	77	77
	T1w/T1wFS/PDw/T2w/IRSE	55	90	86	65	82	81

been reported to show iso- to hypo-intensity of LC (21) as is confirmed in this study. The T2 decrease of LC with increasing field, may explain the low signal intensity of LC on T1w images at 9.4 T. Despite the chosen short TE (2.14 ms), LC has lowest signal, when compared with all other components except calcification. Therefore, TE appears to be more signal limiting than TR for T1w GE images, acquired at 9.4 T. The less efficient depiction of LC with T2w and PDw imaging at 9.4 T may be explained by an increase of T1 for both fibrous tissue and LC at higher field strength, resulting in increased saturation of the fibrous tissue when using TR = 3500 ms.

In carotid artery imaging, FS is generally applied to remove strong signals from peri-adventitious fat which could lead to chemical shift artifacts. We showed that LC was visualized more accurately using GE including FS, when compared with GE without FS. FS is thought to have little impact on tissue contrast within atherosclerotic plaque, because lipids found in atherosclerotic plaque consist primarily of cholesteryl esters and free cholesterol and not triglycerides as in perivascular fat (31). Suppression of the small number of triglycerides in LC with a saturation pulse aimed at the resonant frequency of methylene protons, was surprisingly effective in increasing conspicuity of LC, suggesting an effect on relaxation of nearby water protons.

Contrast-enhanced MRI using small gadolinium chelates has shown capability to differentiate between LC and fibrous cap. Differentiation was evenly possible or better than with T2w imaging (15,32). However in these studies, difference in enhancement between fibrous tissue (~80%) and LC (~30%) occurred by virtue of presence of neovasculature in fibrous tissue (15), which may vary among plaques.

Effect of Resolution on Image Segmentation

There is a relation between resolution of MRI and segmentation results. Some plaque components use little space or are mixed up mostly with another component (area of lipid mingled with fibroblasts). At low resolution, these plaque components cannot be distinguished from each other due to partial volume effects. However, at higher resolution, the partial volume effects will be smaller. Due to the trade-off between signal to noise ratio and resolution, and the lower signal to noise per unit of acquisition time at lower field, prolonged scan times are needed to achieve high resolution at lower field. So, differentiation between small foam cell areas, potentially evolving in LC in near future, and LC, and cell-rich areas may be more practical at higher field strength.

One report suggests that an in vivo in-plane resolution between 156 and 1250 μm per pixel does not impair classification accuracy of human carotid artery plaque components with MRI (33). However, the authors also stated that degradation in resolution is most detrimental to plaques with large numbers of components (33). The thicknesses of tissue layers should at least span one pixel, to differentiate them visually (25). To prevent over-estimation of the surface of spot-like plaque components, the diameter should at least span five pixels (25). Most importantly, one should keep in mind that the classification accuracy depends also on the sizes of component areas delineated on histology. If the delineation of the truth regions has been done in a coarse way, the quality of MR images will also be less demanding.

However, although we have chosen very small truth regions, we have put a mask on the other regions of the carotid plaque and wall layers. We have done this because it would be very time-consuming to categorize the whole plaque and wall area at the resolution of the truth regions. However, higher specificity, sensitivity, and accuracy are easier to achieve this way than for the whole area including more ambiguous regions.

MD-Based Classifier

In this study, segmentation of plaque components was done with a supervised classification algorithm, the "Mahalanobis Distance classifier." Validated automated classification algorithms help in achieving maximum reproducibility and reliability in longitudinal in vivo plaque characterization studies. Variation in shim settings and coil configuration may cause differences in raw signal intensity of the same plaque component between carotid artery samples and modify contrast between two plaque components. Furthermore, display of the image data may vary due to variety of window level settings and will determine the size of the image contrast between two plaque components. Moreover, postprocessing software often applies contrast stretching or normalization which prevents direct comparison of contrast between various MR weightings. Instead of visual assessment, statistics can be applied to the image data which provide a reproducible and quantitative assessment of the image contrast. The slightly better performance of the MD over the ED with respect to detection accuracies of IPH, cell-rich area, and collagen, using the novel panels of MR sequences suggested in this study, suggests the MD classifier to be preferred over the ED classifier for identification of plaque components by MRI.

When the ED was used in earlier reports, the measured distance was largely influenced by contrast weightings with high average signal intensity instead of contrast weightings with highest image contrast (9). Earlier reported automatic plaque segmentation methods using a Gaussian classifier have been successfully applied but needed preprocessing which included rescaling of all pixels values to a baseline "iso-intensity" (34). Others have used specially enhanced cluster analysis (35) or predictive models (36) composed RGB images out of three ex vivo MR sequences by stretching the image contrast of each sequence to an eight-bit color channel. Such a preprocessing step, which can cause loss of data, is not needed in case the MD is used because it is invariant to scaling. However, the segmentation algorithm based on the MD classifier is not as mature as the algorithms that amongst others also take spatial information into account (34–36).

However, the basic segmentation algorithm showed that the MD is preferred over the ED because it is

invariant to scaling and takes into account the covariance among the variables. Therefore, it could be a better metric for comparison of outcomes of various MR weightings than the ED and may compare the same MR weightings obtained at another MR laboratory without influencing classification results. Therefore, classification algorithms based on MD may be used for multicenter trials focused on longitudinal plaque characterization and MD is even suitable for comparison of different imaging modalities (37,38).

Limitations

There are a number of limitations to this study. Clinical in vivo MRI of carotid arteries is complicated by decreased resolution, motion artifacts, signals from flowing blood, and greater spatial variability in MR signal due to the use of surface coils. The automated classification method for detection of plaque components has not been applied to in vivo data in this study.

The acquisition time of the IR-SE sequence was very long and can certainly be shortened by a multislice FSE instead of a single-slice SE approach and the use of phased-array surface coils and multiple receivers. The IR-SE sequence was not compared with the direct thrombus imaging method of Moody et al. (27). For in vivo experiments, incorporation of a double IR module into the IR-SE used in this study will lead to dark blood images. This method might stand the competition with the direct thrombus imaging method of Moody et al. (27) in the in vivo situation; however, this has yet to be studied.

Performance of the classifier needs to be checked for MR images with lower SNR or lower resolution, obtained within clinically realistic acquisition times. Lower resolution will come with shorter acquisition times at the same SNR. At the high in-plane resolution in this study, the truth regions chosen with scrutinized microscopy were also very small. Perfect matching between histology and MRI is always difficult, but with the small truth regions used in this study it even became more challenging. Furthermore, the sample size was limited and so was the number of carotid artery sections with IPH. Only old IPH and not fresh/recent IPH were found in this data set because the carotid artery samples were not obtained from surgery but from autopsy. Second, due to the small number of carotid artery sections, a real classification experiment using an independent training set and test set could not be performed. Instead, automatic segmentation based on adjacent slices of the same carotid artery sample and segmentation based on a combination of slices from different carotid artery samples was performed. Third, because of the use of novel sequences and the small number of carotid samples, automatic segmentation was only performed for small regions corresponding to histological truth regions and not for the entire plaque. To verify the ability of the automated classification method to characterize also regions with ambiguity with respect to the type of plaque component, additional research is needed using a larger number of carotid artery samples.

CONCLUSIONS

In conclusion, identification of LC and IPH in human carotid artery plaque was improved ex vivo at 9.4 T with two clinically not commonly used MRI techniques, T1w GE with FS and IR-SE (TI = 1000 ms). Results of in vivo application of these MRI techniques will have to be awaited. Automatic plaque segmentation using a supervised classification algorithm based on the MD was feasible and led to slightly better accuracy of identification of IPH, cell-rich area, and collagen, showing promise for the MD metric in multicenter trials on longitudinal plaque characterization.

REFERENCES

1. Pasterkamp G, Schoneveld AH, van der Wal AC, Haudenschild CC, Clarijs RJ, Becker AE, Hillen B, Borst C. Relation of arterial geometry to luminal narrowing and histologic markers for plaque vulnerability: the remodeling paradox. J Am Coll Cardiol 1998;32:655–662.
2. Falk E, Shah PK, Fuster V. Coronary plaque disruption. Circulation 1995: 92:657–671.
3. Ross R. Atherosclerosis is an inflammatory disease. Am Heart J 1999; 138:S419–S420.
4. Chu B, Kampschulte A, Ferguson MS, Kerwin WS, Yarnykh VL, O'Brien KD, Polissar NL, Hatsukami TS, Yuan C. Hemorrhage in the atherosclerotic carotid plaque: a high-resolution MRI study. Stroke 2004;35:1079–1084.
5. Kampschulte A, Ferguson MS, Kerwin WS, Polissar NL, Chu B, Saam T, Hatsukami TS, Yuan C. Differentiation of intraplaque versus juxtaluminal hemorrhage/thrombus in advanced human carotid atherosclerotic lesions by in vivo magnetic resonance imaging. Circulation 2004;110:3239–3244.
6. Takaya N, Yuan C, Chu B, Saam T., Polissar NL, Jarvik GP, Isaac C, McDonough J, Natiello C, Small R, Ferguson MS, Hatsukami TS. Presence of intraplaque hemorrhage stimulates progression of carotid atherosclerotic plaques: a high-resolution magnetic resonance imaging study. Circulation 2005;111:2768–2775.
7. Toussaint JF, Southern JF, Fuster V, Kantor HL. T2-weighted contrast for NMR characterization of human atherosclerosis. Arterioscler Thromb Vasc Biol 1995;15:1533–1542.
8. Toussaint JF, Southern JF, Fuster V, Kantor HL. Water diffusion properties of human atherosclerosis and thrombosis measured by pulse field gradient nuclear magnetic resonance. Arterioscler Thromb Vasc Biol 1997;17:542–546.
9. Clarke SE, Hammond RR, Mitchell JR, Rutt BK. Quantitative assessment of carotid plaque composition using multicontrast MRI and registered histology. Magn Reson Med 2003;50:1199–1208.
10. Clarke SE, Beletsky V, Hammond RR, Hegele RA, Rutt BK. Validation of automatically classified magnetic resonance images for carotid plaque compositional analysis. Stroke 2006;37:93–97.
11. Rogers WJ, Prichard JW, Hu YL, Olson PR, Benckart DH, Kramer CM, Vido DA, Reichek N. Characterization of signal properties in atherosclerotic plaque components by intravascular MRI. Arterioscler Thromb Vasc Biol 2000;20:1824–1830.
12. Cai JM, Hatsukami TS, Ferguson MS, Small R, Polissar NL, Yuan C. Classification of human carotid atherosclerotic lesions with in vivo multicontrast magnetic resonance imaging. Circulation 2002;106: 1368–1373.
13. Cai J, Hatsukami TS, Ferguson MS, Kerwin WS, Saam T, Chu B, Takaya N, Polissar NL, Yuan C. In vivo quantitative measurement of intact fibrous cap and lipid-rich necrotic core size in atherosclerotic carotid plaque: comparison of high-resolution, contrast-enhanced magnetic resonance imaging and histology. Circulation 2005;112: 3437–3444.
14. Mitsumori LM, Hatsukami TS, Ferguson MS, Kerwin WS, Cai J, Yuan C. In vivo accuracy of multisequence MR imaging for identifying unstable fibrous caps in advanced human carotid plaques. J Magn Reson Imaging 2003;17:410–420.
15. Yuan C, Kerwin WS, Ferguson MS, Polissar NL, Zhang S, Cai J, Hatsukami TS. Contrast-enhanced high resolution MRI for atherosclerotic carotid artery tissue characterization. J Magn Reson Imaging 2002;15:62–67.

16. Yuan C, Mitsumori LM, Ferguson MS, Polissar NL, Echelard NL, Ortiz G, Small R, Davies JW, Kerwin WS, Hatsukami TS. In vivo accuracy of multispectral magnetic resonance imaging for identifying lipid-rich necrotic cores and intraplaque hemorrhage in advanced human carotid plaques. Circulation 2001;104:2051–2056.
17. Saam T, Hatsukami TS, Takaya N, Chu B, Underhill H, Kerwin WS, Cai J, Ferguson MS, Yuan C. The vulnerable, or high-risk, atherosclerotic plaque: noninvasive MR imaging for characterization and assessment. Radiology 2007;244:64–77.
18. Mitchell DG. Preparatory pulses, including fat suppression. In: Mitchell DG, editor. MRI principles, 2nd ed. Philadelphia: Saunders; 2004. pp 177–198.
19. Vinitski S, Consigny PM, Shapiro MJ, Janes N, Smullens SN, Rifkin MD. Magnetic resonance chemical shift imaging and spectroscopy of atherosclerotic plaque. Invest Radiol 1991;26:703–714.
20. Trouard TP, Altbach MI, Hunter GC, Eskelson CD, Gmitro AF. MRI and NMR spectroscopy of the lipids of atherosclerotic plaque in rabbits and humans. Magn Reson Med 1997;38:19–26.
21. Te Boekhorst BC, Cramer MJ, Van Oosterhout MF, Pasterkamp G, Doevendans PA, Van Echteld CJ. High-resolution MRI for identification of various components of human carotid artery plaque using different weightings and fat suppression. J Cardiovasc Magn Reson 2007;9:252–253.
22. Babiloni F, Bianchi L, Semeraro F, del R Millan J, Mourino J, Cattini A, Salinari S, Marciani MG, Concotti F. Mahalanobis Distance-Based Classifiers Are Able to Recognize EEG Patterns by Using Few EEG Electrodes. In: Proceedings 23rd Annual Conference IEEE/EMBS, Istanbul, Oct.25–28, 2001.
23. Dalager-Pedersen S, Falk E, Ringgaard S, Kristensen IB, Pedersen EM. Effects of temperature and histopathologic preparation on the size and morphology of atherosclerotic carotid arteries as imaged by MRI. J Magn Reson Imaging 1999;10:876–885.
24. Morrisett J, Vick W, Sharma R, Lawrie G, Reardon M, Ezell E, Schwartz J, Hunter G, Gorenstein D. Discrimination of components in atherosclerotic plaques from human carotid endarterectomy specimens by magnetic resonance imaging ex vivo. Magn Reson Imaging 2003;21:465–474.
25. Schar M, Kim WY, Stuber M, Boesiger P, Manning WJ, Botnar RM. The impact of spatial resolution and respiratory motion on MR imaging of atherosclerotic plaque. J Magn Reson Imaging 2003;17:538–544.
26. Shinnar M, Fallon JT, Wehrli S, Levin M, Dalmacy D, Fayad ZA, Badimon JJ, Harrington M, Harrington E, Fuster V. The diagnostic accuracy of ex vivo MRI for human atherosclerotic plaque characterization. Arterioscler Thromb Vasc Biol 1999;19:2756–2761.
27. Moody AR, Murphy RE, Morgan PS, Martel AL, Delay GS, Allder S, MacSweeney ST, Tennant WG, Gladman J, Lowe J, Hunt BJ. Characterization of complicated carotid plaque with magnetic resonance direct thrombus imaging in patients with cerebral ischemia. Circulation 2003;107:3047–3052.
28. Murphy RE, Moody AR, Morgan PS, Martel AL, Delay GS, Allder S, MacSweeney ST, Tennant WG, Gladman J, Lowe J, Hunt BJ. Prevalence of complicated carotid atheroma as detected by magnetic resonance direct thrombus imaging in patients with suspected carotid artery stenosis and previous acute cerebral ischemia. Circulation 2003;107:3053–3058.
29. Toussaint JF, Pachot-Clouard M, Kantor HL. Tissue characterization of atherosclerotic plaque vulnerability by nuclear magnetic resonance. J Cardiovasc Magn Reson 2000;2:225–232.
30. Honda M, Kitagawa N, Tsutsumi K, Nagata I, Morikawa M, Hayashi T. High-resolution magnetic resonance imaging for detection of carotid plaques. Neurosurgery 2006;58:338–346.
31. Yuan C, Kerwin WS. MRI of atherosclerosis. J Magn Reson Imaging 2004;19:710–719.
32. Wasserman BA, Smith WI, Trout HH, Cannon RO, Balaban RS, Arai AE. Carotid artery atherosclerosis: in vivo morphologic characterization with gadolinium-enhanced double-oblique MR imaging initial results. Radiology 2002;223:566–573.
33. Ronen RR, Clarke SE, Hammond RR, Rutt BK. Resolution and SNR effects on carotid plaque classification. Magn Reson Med 2006;56:290–295.
34. Liu F, Xu D, Ferguson MS, Chu B, Saam T, Takaya N, Hatsukami TS, Yuan C, Kerwin WS. Automated in vivo segmentation of carotid plaque MRI with morphology-enhanced probability maps. Magn Reson Med 2006;55:659–668.
35. Itskovich VV, Samber DD, Mani V, Aguinaldo JG, Fallon JT, Tang CY, Fuster V, Fayad ZA. Quantification of human atherosclerotic plaques using spatially enhanced cluster analysis of multicontrast-weighted magnetic resonance images. Magn Reson Med 2004;52:515–523.
36. Anderson RW, Stomberg C, Hahm CW, Mani V, Samber DD, Itskovich VV, Valera-Guallar L, Fallon JT, Nedanov PB, Huizenga J, Fayad ZA. Automated classification of atherosclerotic plaque from magnetic resonance images using predictive models. Biosystems 2007;90:456–466.
37. Silveira L Jr, Sathaiah S, Zangaro RA, Pacheco MT, Chavantes MC, Pasqualucci CA. Correlation between near-infrared Raman spectroscopy and the histopathological analysis of atherosclerosis in human coronary arteries. Lasers Surg Med 2002;30:290–297.
38. Nogueira GV, Silveira L, Martin AA, Zangaro RA, Pacheco MT, Chavantes MC, Pasqualucci CA. Raman spectroscopy study of atherosclerosis in human carotid artery. J Biomed Opt 2005;10:031117.